



## Non-dimensional scaling of tidal stream turbines

A. Mason-Jones<sup>a</sup>, D.M. O'Doherty<sup>a,\*</sup>, C.E. Morris<sup>a</sup>, T. O'Doherty<sup>a</sup>, C.B. Byrne<sup>a</sup>, P.W. Prickett<sup>a</sup>,  
R.I. Grosvenor<sup>a</sup>, I. Owen<sup>b</sup>, S. Tedds<sup>b</sup>, R.J. Poole<sup>b</sup>

<sup>a</sup>School of Engineering, Queen's Buildings, Cardiff University, The Parade, Cardiff, CF24 3AA, UK

<sup>b</sup>School of Engineering, University of Liverpool, UK

### ARTICLE INFO

#### Article history:

Received 21 November 2011

Received in revised form

4 May 2012

Accepted 7 May 2012

Available online 10 June 2012

#### Keywords:

Marine turbines

Scaling

CFD

Torque coefficient

Power coefficient

Thrust coefficient

Velocity profile

### ABSTRACT

The impact of local depth-wise velocity profiles on tidal turbine performance is important. Although the use of standard power laws for predicting velocity profiles is common, these laws may underestimate the magnitude of the depth-wise velocity shear and power attenuation. Predicting the performance of a tidal turbine in a high velocity shear is crucial in terms of power extraction. This paper discusses the dimensional scaling of a turbine using CFD and experimental data. Key performance characteristics (power, torque and thrust coefficients) were studied with increasing diameters and velocities, by generating a series of non-dimensional curves. This provides a first order approximation for matching turbine performance characteristics to site conditions. The paper also shows that the use of a volume-averaged velocity derived from the upstream velocity profile can be used to determine these key performance characteristics. These are within 2% of those determined assuming a uniform flow. The paper also shows that even changes in the blade pitch angle results in new turbine characteristics under uniform velocity conditions and it is expected that these can be used for profiled flow.

© 2012 Elsevier Ltd. All rights reserved.

### 1. Introduction

Tidal stream technology is now developing apace, different turbine designs are being proposed, and experimental performance testing is being carried out at small scale [1,2], with additional support from Computational Fluid Dynamics (CFD) [3,4]. As with all model testing in fluid mechanics, there is the issue of how to translate the results from the experimental to the full scale. The scaling is conventionally done using non-dimensional analysis, and the purpose of this paper is to demonstrate the effectiveness of such an analysis when applied to a Horizontal Axis Tidal Stream Turbine (HATT) with a particular emphasis on how to deal with the characteristic velocity when the turbine is exposed to a non-uniform inlet velocity profile.

When deploying HATTs, it was suggested over a decade ago by Bryden et al. [5] that where shipping restrictions exist, the tip of the rotor needs to be 1.5 m below the lowest astronomical tide (LAT) for the lowest negative storm surge, another 2.5 m for the trough of a 5 m wave and a further 5 m to minimise the potential for damage from local shipping lanes. Therefore, the tip of a HATT at top dead centre should be around 9 m below LAT. It has also been recommended that the bottom of the HATT should not be within 25% of

the water depth at LAT from the seabed due to the high shear levels at these depths [6]. However this 25% restriction on the distance between the seabed and rotor tip may not be practical at locations where large cargo vessels are common place, such as within the Severn Estuary where vessel drafts of approximately 14 m are typical and the maximum available depth is 35 m [7].

Although the Severn Estuary is not currently one of the prime sites for deploying tidal stream turbines, it may be an important part of the UK's tidal stream resource in the future, due to its ability to mitigate problems associated with power variability from out of phase tidal cycles and power variability. In fact, it has been shown that with the installation of tidal stream devices located in the Severn Estuary along with further installations in the Clyde, Tees, Humber, Menai Straits and the Mersey, a regular National grid supply could be established [8].

The DTI report on the economic viability of a simple tidal stream energy capture device [9], and UK resource estimates from Black and Veatch [10] suggest that typical water depths at the suitable sites around the UK range from 25 to 40 m and that consequently the corresponding recommended rotor diameter is between 10 m and 20 m. However, as device deployment expands into large arrays, additional placement restrictions from local water depths and/or shipping may arise. As such, it is likely that some turbines will need to be placed within 25% of the water depth at LAT from the seabed to maximise the power generated.

\* Corresponding author. Tel.: +44 0 29 2087 4542; fax: +44 0 29 2087 4597.  
E-mail address: [odohertydm@cf.ac.uk](mailto:odohertydm@cf.ac.uk) (D.M. O'Doherty).

Nomenclature			
$A$	swept area of the turbine ( $m^2$ )	$T$	torque generated by the flow (Nm)
$C_P$	power coefficient	TSR	tip speed ratio
$C_T$	thrust coefficient	unc	uncorrected performance characteristic
$C_\theta$	torque coefficient	$U_F$	unbounded free stream velocity in the water flume (m/s)
$D$	diameter (m)	$U_T$	free stream velocity in the water flume (m/s)
$F$	axial thrust or force generated (N)	$U_T/U_F$	blockage correction factor
$H$	height from seabed to turbine rotational centre (m)	$V$	velocity (m/s)
HATT	horizontal axis tidal turbine	$V_d$	depth-averaged velocity (m/s)
$P$	power generated (W)	$V_v$	volume-averaged velocity (m/s)
$R$	radius of turbine (m)	$\rho$	density ( $kg/m^3$ )
$Re$	Reynolds number	$\omega$	angular velocity (rad/s)
RSM	Reynolds Stress Model	$\mu$	dynamic viscosity (Pa s)

To date, most studies predicting the power characteristics for a tidal stream turbine have assumed an idealised water flow with a uniform velocity profile. However, in reality the velocity distribution will be profiled and, as shown in Fig. 1, since the power is related to the cube of the upstream velocity, the available power is biased towards the surface so that typically 75% of the available power is in the upper 50% of the water column [6].

The nature of the velocity profile through the water depth is dependent on factors such as local bathymetry and turbulence. For the velocity profile, the use of the 1/7th or 1/10th power law is typically accepted throughout the wind industry and the emerging tidal energy sector alike. However actual velocity profiles can be very different and it is important to understand how model-scale performance characteristics can be scaled to account not only for different water velocities and turbine sizes, but to also account for a non-uniform velocity profile.

## 2. Non-dimensional analysis

Consider a turbine of a given geometry with a characteristic diameter  $D$ , rotating with an angular velocity  $\omega$ , while immersed in a fluid of density  $\rho$ , dynamic viscosity  $\mu$ , moving with a characteristic velocity  $V$ . The power output from the turbine is therefore a function,  $f$ , of these variables:

$$P = f(D, \omega, \rho, \mu, V) \quad (1)$$

The relationship between the power and the other variables can be expressed, using the Buckingham Pi theory, through three non-dimensional groups:

$$\frac{P}{\rho D^2 V^3} = f\left(\frac{\rho V D}{\mu}, \frac{\omega D}{V}\right) \quad (2)$$

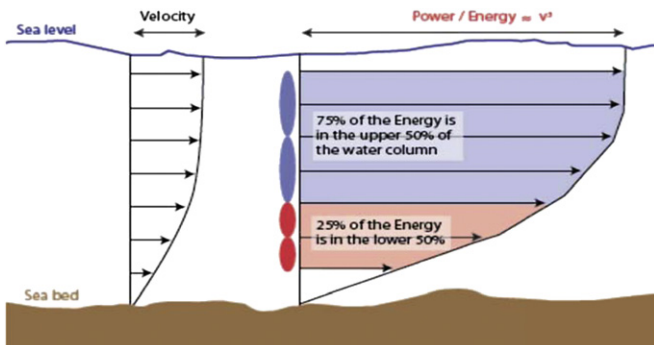


Fig. 1. Velocity and power distribution through water column [6].

These groupings are more conventionally expressed as the Power Coefficient:

$$C_P = \frac{P}{\frac{1}{2} \rho A V^3} \quad (3)$$

Reynolds number:

$$Re = \frac{\rho V D}{\mu} \quad (4)$$

and Strouhal number or, conventionally for rotating machinery, Tip-Speed-Ratio: TSR:

$$TSR = \frac{\omega R}{V} \quad (5)$$

The inclusion of constants such  $\frac{1}{2}$  and  $\pi$  do not of course change the dimensionless form of the groups, they just allow them to be expressed in a more conventional engineering format. For example, the power coefficient as written in equation (3) is the ratio of the actual power output to the kinetic power available in the fluid approaching the swept area of the turbine.

Therefore the relationship now becomes:

$$C_P = f(Re, TSR) \quad (6)$$

A similar non-dimensional analysis for the torque,  $T$ , and the axial thrust on the turbine,  $F$ , will lead to torque and thrust coefficients,  $C_\theta$  and  $C_T$ :

$$C_\theta = \frac{T}{\frac{1}{2} \rho A R V^2} \quad (7)$$

$$C_T = \frac{F}{\frac{1}{2} \rho A V^2} \quad (8)$$

and

$$C_\theta = f_1(Re, TSR) \quad (9)$$

$$C_T = f_2(Re, TSR) \quad (10)$$

The functions  $f, f_1$  and  $f_2$  can be determined experimentally or, as shown later in the paper, by CFD, and, provided the same  $Re$  and  $TSR$  are used in the model and the full scale, the values for  $C_P, C_\theta$  and  $C_T$  of the turbine in the full scale will be the same as that measured or predicted using the model. It is worth noting, and it is

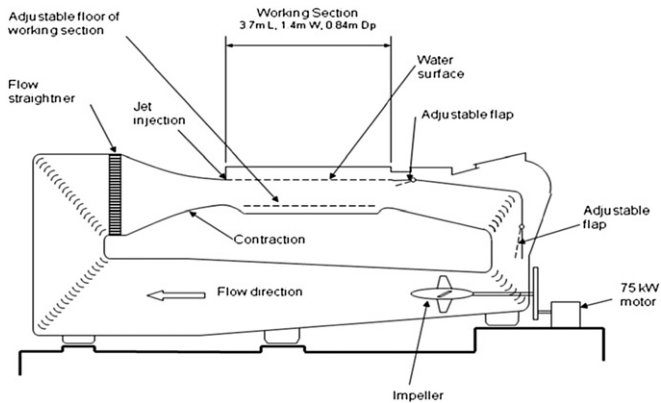


Fig. 2. Water flume schematic.

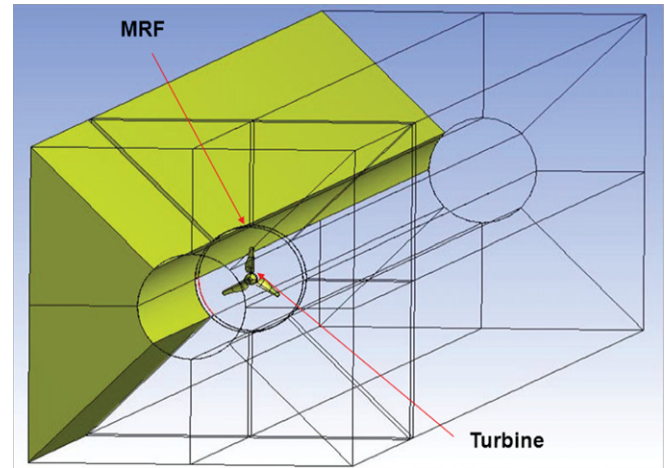


Fig. 4. CFD reference model.

investigated within this paper, that in high Reynolds number flows (i.e.  $Re$  of the order  $10^6$ ) it is not unusual for the independent variable group to become independent of Reynolds number, which simplifies significantly the scaling process.

In this paper the performance of a HATT will be investigated using CFD, for different uniform inlet velocities and a range of turbine diameters, to demonstrate the effect on the power and torque coefficients of changing Reynolds number. The experimental data obtained from a 0.5 m diameter HATT in a water flume and corrected for blockage, will also be included for validation purposes. The CFD will then be used to investigate the effect of a realistic non-uniform velocity profile on the output characteristics of the turbine and how, in such a case, the characteristic velocity should be represented. Finally, the geometry of the turbine will be changed by setting the turbine blades at different angles of attack, to demonstrate the effect of not maintaining geometric similarity.

### 3. Experimental testing

Testing was undertaken in the recirculating water flume at the University of Liverpool. The flume utilises a 75 kW motor-driven axial-flow impeller to circulate 80 000 L of water. The water flows into the working section which is 3.7 m long by 1.4 m wide with a depth of 0.85 m, Fig. 2.

To ensure flow uniformity, a honeycomb and contraction guide vanes are used prior to the water entering the working section. When testing a model turbine it is important to have an accurate measure of the upstream velocity as it can change as the rotational speed of the turbine is allowed to vary during testing. Detailed

Laser Doppler Anemometry measurements in the flume have shown the free stream turbulence to be typically 3%, although it does vary with water speed. When the flume is used with its free surface configuration the contraction ensures a mostly uniform velocity across the section with only thin boundary layers on the solid surfaces ( $\sim 16$  mm at the middle of the working section). To ensure there is no velocity deficit at the free surface, the surface flow, which is retarded by the walls of the contraction is re-energised using a thin jet which is added to the surface flow as it emerges from the contraction. The position of the jet is indicated on Fig. 2; the nozzle spans the width of the flume and is 1 mm high. The appropriate speed of the jet injection is known from previous calibrations. For model HATT testing, the working section was set to be an open flume, allowing the model turbine to be supported from above on a cross-beam.

The majority of model testing that has been reported to date has assumed that the power coefficient is independent of Reynolds number, although Batten et al. [11] do recognise the significance of  $Re$  in the selection of an 800 mm diameter HATT. Fig. 3 shows the 0.5 m diameter HATT used for the experimental tests. The important factor that has to be taken into account when testing a model turbine in the confines of a water flume is the blockage effect, whose correction is described in detail by others [12,13]. The data that has been corrected for blockage, and discussed in this paper, are for the turbine operating with an optimal blade pitch angle, of  $6^\circ$  measured at the chord of the blade tip, to extract the maximum power. The centre of the turbine was located at a depth of 0.425 m, midway along the working section. The turbine was connected to

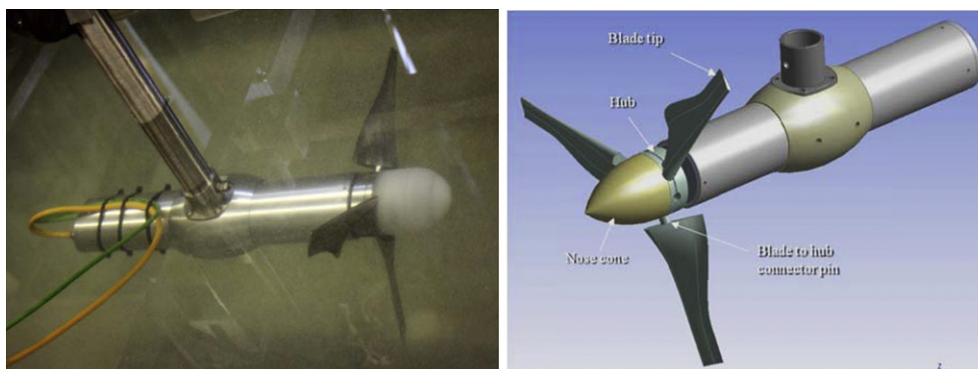


Fig. 3. The 0.5 m diameter prototype turbine in test flume and graphic representation.

**Table 1**  
Meshing schemes for turbine faces.

Meshing scheme no	Up and downstream edge length scale	Rectangular channel cell no	Turbine MRF cell no	% Of grid independence
Face key	Zone	Zone	zone	
Tip-middle-root-hub		2	3	
1	40-60-40-80	89533	278327	91
2	30-40-30-60	89533	512473	96
3	20-30-20-60	89533	740903	98
4	20-30-20-50	89533	969332	99
5	20-20-20-40	89533	1239038	99
6	20-20-20-30	89533	1494921	100
7	15-20-20-40	89533	1750803	100

a Baldor brushless AC servo-motor in order to measure/calculate the torque, angular velocity and power generated via hydrodynamic loading. A regen resistor or dynamic brake was used to apply an opposing load to that developed by the hydrodynamic forces from the turbine. This was combined with a control system which in turn was programmed via a computer.

For each experiment the flume was set to the desired free stream velocity and the turbine allowed to free-wheel (i.e. zero nominal torque applied) before a resistive torque (proportional to the drive-rated current of the servo-motor) was applied and the rotation speed logged for 30 s. This process was repeated until the peak current was reached and servo-motor cut-out occurred (2.82 A or a peak torque of approximately 2.3 Nm). Thus each experiment progressed from high values of the tip speed ratio to some lower value which varied depending on the power extraction. Therefore at higher flume speeds cut-out occurred at lower values of the dimensionless power coefficient and it was not always possible to determine the peak CP values [2].

The thrust on the turbine operating in the flume was determined experimentally using a 50 kg strain gauge force block, the design of which is described in detail in [14]. The force block, located at the point at which the turbine stanchion was clamped, was calibrated by applying a load with an Instron model 5582 machine. Loads were applied from 5 kg to 50 kg in steps of 5 kg. The force block was found to have an accuracy of about 1%.

The TSR,  $C_p$ ,  $C_\theta$  and  $C_T$  presented are corrected for blockage effects. To determine the blockage factor ( $U_T/U_F$ ) [13], an actuator disc model of the flow through the turbine was used. Two assumptions are made when calculating the blockage factor: the flow across any cross section of the area enclosing the turbine is uniform and there is a pressure drop across the turbine in the direction of the flow [15]. The equations 11–14, are solved using an

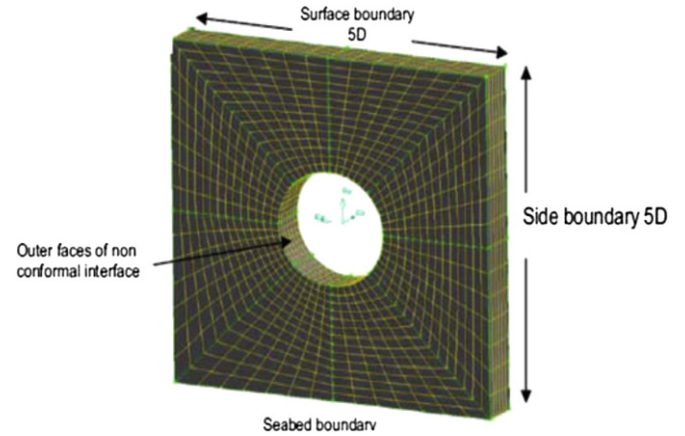


**Fig. 6.** Width and depth of reference CFD model.

iterative process to calculate the blockage factor. The corrections applied to the TSR,  $C_p$ ,  $C_\theta$  and  $C_T$  respectively are as follows:

$$C_p = C_{p \text{ unc}} (U_T/U_F)^3 \tag{11}$$

$$C_\theta = C_{\theta \text{ unc}} (U_T/U_F)^2 \tag{12}$$

$$C_T = C_{T \text{ unc}} (U_T/U_F)^2 \tag{13}$$

$$\text{TSR} = \text{TSR}_{\text{unc}} (U_T/U_F) \tag{14}$$

Full details of the experimental analysis of the flume data used in this paper are given in [2].

**4. CFD modelling of a horizontal axis tidal turbine**

The operational performance characteristics of a HATT were obtained using a series of quasi-static CFD models for different size turbines, using techniques published previously [7]. All the turbines discussed in this paper, including the experimental 3 bladed turbine, utilised a Wortmann FX 63-137 profile, with a 33° twist from the blade root to tip [16]. The Reynolds Stress Model (RSM) was used to close the Navier–Stokes equations.

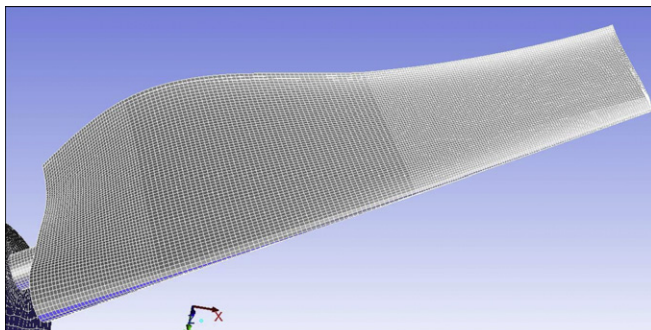


**Fig. 5.** Optimum meshing scheme used in study.

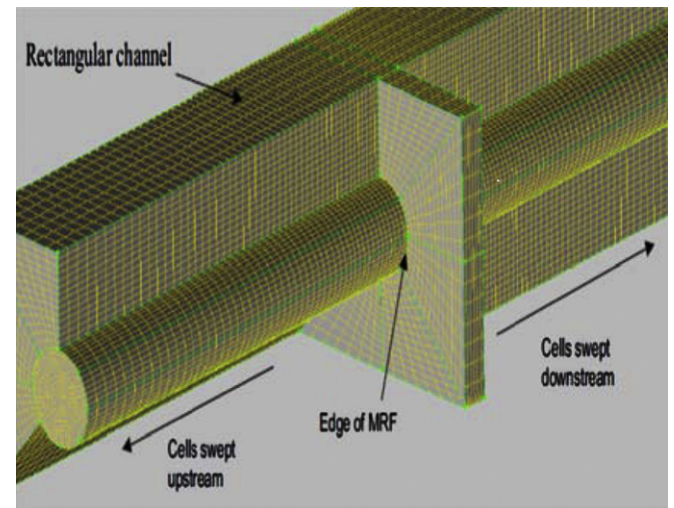


**Fig. 7.** Swept faces forming rectangular sea flume (not showing MRF volume).

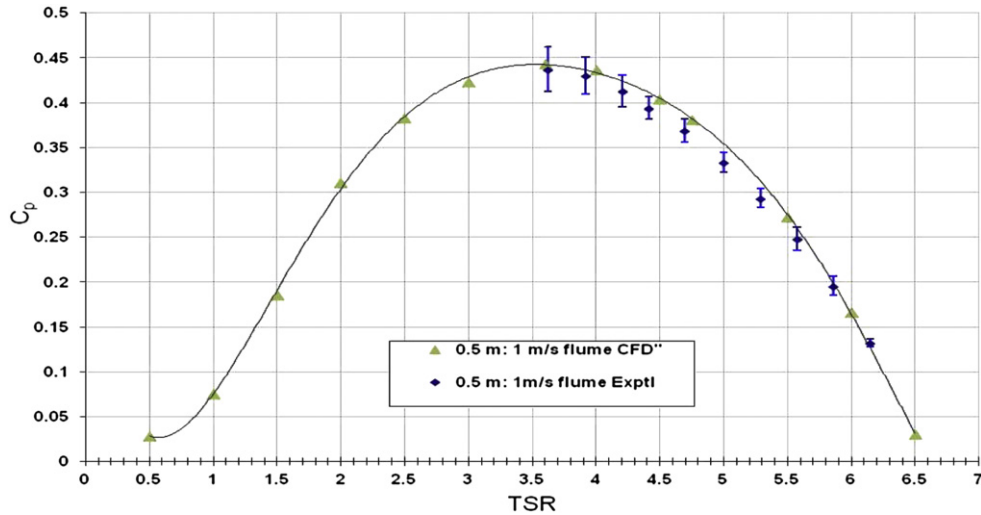


Fig. 8. Comparison of measured power output and that predicted by CFD.

The CFD domain was defined with a square cross-section  $5D \times 5D$  and a downstream length of  $40D$  to ensure the turbine was fully isolated from any boundary effects, and the turbine was centred within the domain cross-section, and located  $10D$  downstream from the inlet boundary [16], Fig. 4. To simulate rotation, the HATT was subtracted from a cylindrical volume which formed the basis for a Moving Reference Frame (MRF) [17]. Eight volumes were then created around the circumference of the cylinder so that their inner faces formed a non-conformal interface with the circumferential face of the cylinder. To limit poor numerical diffusion near the non-conformal interface and the tips of each blade, a clearance of 50% of blade length was used. Various meshing schemes were developed for the blade and hub surfaces to determine an appropriate mesh density for the MRF.

Table 1 shows the meshing schemes used to mesh the HATT. The upstream and downstream edge lengths for each blade surface were varied in accordance with defined cell spacing, e.g. (20–30–20–50) (Fig. 5). From Table 1 meshing scheme No. 4 gave the preferred balance between numerical solution time and grid dependency and was therefore used in all subsequent models. This model provided a compromise between a poor mesh which converged in 4 h and a time of 8 h for scheme 4 and 10 h for scheme 7, for every TSR examined. Although there was good agreement between the CFD and measured data, grid independency considerations also resulted

in a compromise in the magnitude of the  $y^+$  term ( $y^+ \sim 300$ ). It was also found that the distribution of the  $y^+$  over the blade was as important as its magnitude. Further descriptions of the grid checks and suitability for modelling the turbines are described by Mason-Jones [16].

The volumes surrounding the MRF were meshed using quadrilateral cells with a node successive ratio of 1.016 biased toward the front and rear faces of the MRF, Figs. 6 and 7. A rectangular domain was then created by sweeping the faces of the rectangular volumes surrounding the MRF up- and down-stream by  $10D$  and  $40D$ , respectively.

The mesh for the rectangular domain was also created during extrusion and controlled via a mesh line with a node successive ratio of 1.016 biased toward the MRF volume, Fig. 7. Two further faces were created on the up- and down-stream location of the MRF and were meshed using a tiled scheme. Each face was then swept to the same length as the previously discussed volumes forming two cylinders with the same lengthwise successive ratio. Through the use of a User Defined Function angular velocity sweeps, for each configuration, produced a set of torque and power curves.

Having established the CFD analytical process, the power and torque characteristics were obtained for geometrically similar turbines having diameters of 10, 15, 20 and 30 m, and for a uniform inlet flow velocity of 3.08 m/s (6 knots). In addition, the effects of

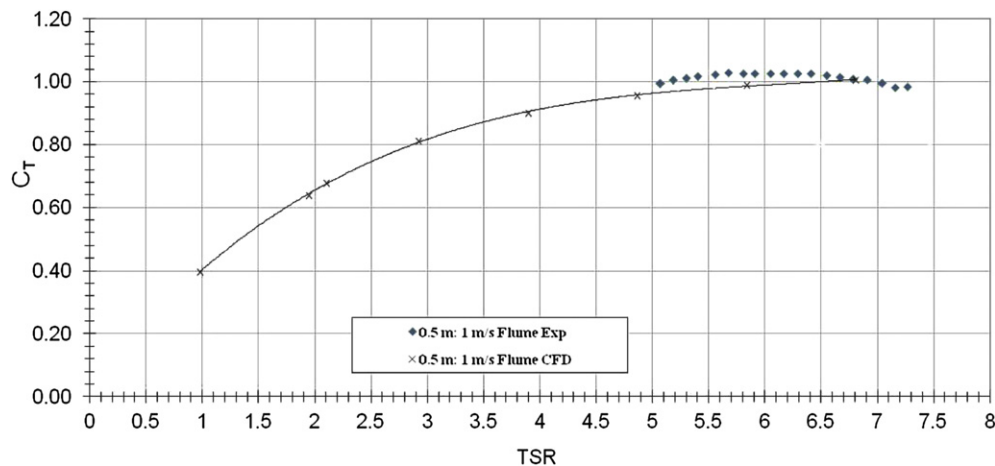


Fig. 9. Comparison of measured thrust and that predicted by CFD.

upstream velocity were also investigated by modelling a range of velocities from 1 m/s to 3.08 m/s for the 10 m diameter turbine. The CFD model of the 10 m diameter turbine was also used to evaluate the effects of varying the turbine geometry by modelling the flow with the blades set at an angle of 0°, 3°, 9°, and 12° in addition to the standard 6° as used in all the other models.

The configuration of the 0.5 m diameter experimental turbine in the water flume was also modelled. The CFD models for the experimental testing of the 0.5 m turbine were set up in the same way as described in the previous section, but with the outer domain being the same size as the water flume. The downstream length, including the curvature of the water flume, prior to the axial-flow impeller, was modelled as an 8D straight length. The 0.5 m turbine (6° blade pitch angle) was located centrally within the cross-section and 4D from the inlet boundary. The upper surface was assigned as a solid frictionless boundary, and both the CFD and the experiments can be expected to have blockage effects included.

#### 4.1. Performance assessment of a HATT using CFD

The measured output from the experimental turbine in the flume is shown in Fig. 8, alongside that from the CFD. The conditions for the data shown are for 1 m/s uniform velocity profile, which gives a Reynolds number of  $5 \times 10^5$ , based on the turbine diameter.

Fig. 8 shows  $C_p$  curves for a set of flume experimental data and a flume CFD model. Both sets of data are raw and uncorrected for blockage. Whilst the experimental set-up was limited, based on the level of torque that could be generated by the servo-motor, the data provided peak operating conditions for the turbine. What is clear is that the coefficient curves, (measured and simulated), show a good correlation to each other. The experimental data also shows the error bars associated with the  $C_p$  magnitude which shows a maximum spread of data of  $\pm 5\%$ . The comparison to the best line fit applied to the CFD data provides confidence in the predicted values.

Fig. 9 shows the  $C_T$  curves, again for both experimental and CFD data sets. The experimental data shown are for the peak thrust values which occur at the high end of the TSR (i.e. near free-wheeling). The area of interest for the thrust measurements was concentrated on the peak values since this is the area of particular interest for structural designers. Once again the data show good correlation with the CFD data and the best line fit.

From literature, the typical size and power rating for current tidal stream designs ranges between diameters of 6 m and 20 m with power ratings between 250 kW and 2 MW. A 2007 DTI report

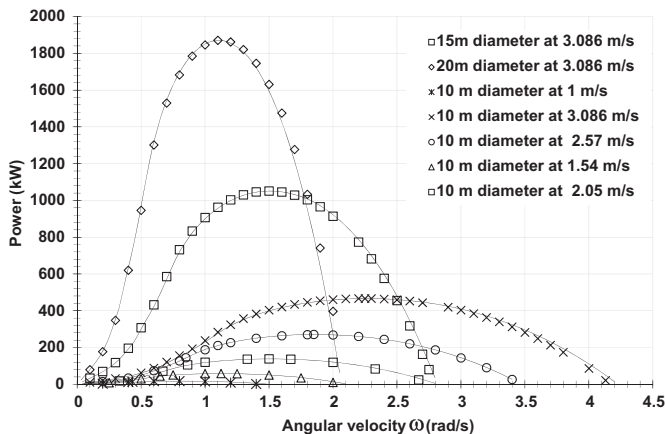


Fig. 10. Power curves with varying diameter and flow velocity.

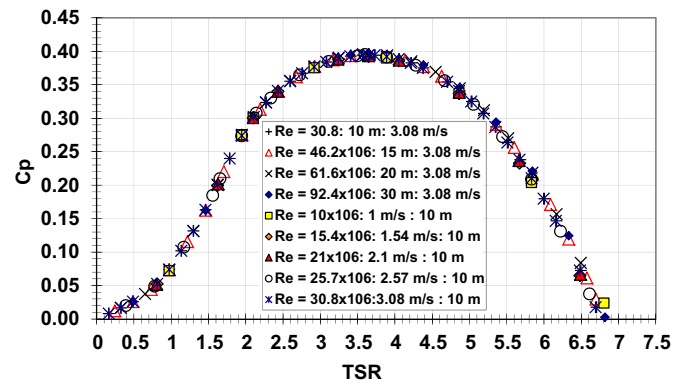


Fig. 11. Combined power coefficient ( $C_p$ ) vs TSR with increasing turbine diameter and upstream water velocity (uniform flow = 3.08 m/s for diameters 10 m–30 m).

[9], on the economic viability of tidal stream energy capture devices discusses a number of device developers and the ratings of their proposed designs. Several of these devices are being developed or have been installed as full scale prototypes with typical turbine diameters of up to 20 m and a typical power rating of 1 MW. The devices are rated with a tidal velocity of typically 2.5 m/s, however they will be operating at a range of hydrodynamic conditions, i.e. tidal range velocities, velocity profiles, etc.

The CFD techniques described in the previous section have been used to calculate the power output and axial thrust for a turbine for a range of diameters and different uniform inlet velocities. For example, in Fig. 10 the power output is shown for turbine diameters of 10, 15 and 20 m, for an inlet velocity of 3.08 m/s, and for a 10 m diameter turbine with inlet velocities of 3.08, 2.57, 2.05 and 1.54 m/s. All the blade angles in this case are 6°. Presenting the data in this way is useful from an engineering point of view as the actual values of power and shaft rotational speed can be seen for the different flow velocities and turbine sizes. However, as seen earlier in equation (6), the non-dimensional analysis shows that the dimensionless power is a function of Reynolds number and Tip-Speed Ratio.

Fig. 11 shows  $C_p$  vs TSR for the CFD models for the same values of turbine diameters and uniform water velocities as the data in Fig. 8; that is, for a wide range of Reynolds number. It can be seen that the data collapses to a single curve, showing that the power coefficient is not sensitive to Reynolds number at these high values. Therefore, for a turbine of this geometry, for a range of sizes and water velocities, the peak power coefficient is predicted by the CFD to be 0.4, and to occur at a TSR of about 3.6.

Similarly, Figs. 12 and 13 show that plotting the dimensionless torque and axial thrust coefficients,  $C_Q$  and  $C_T$  (respectively) against

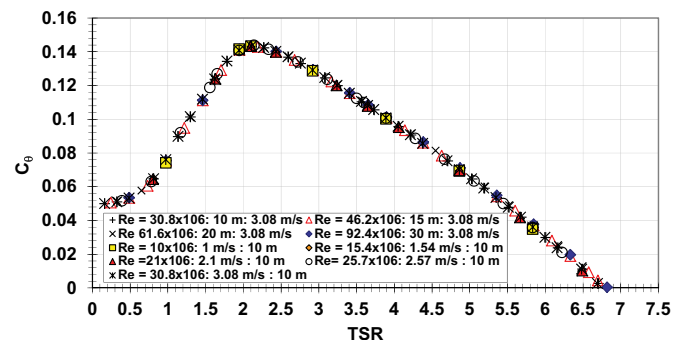


Fig. 12. Combined torque coefficient ( $C_Q$ ) vs TSR with increasing turbine diameter and upstream water velocity (uniform flow = 3.08 m/s for diameters 10 m–30 m).

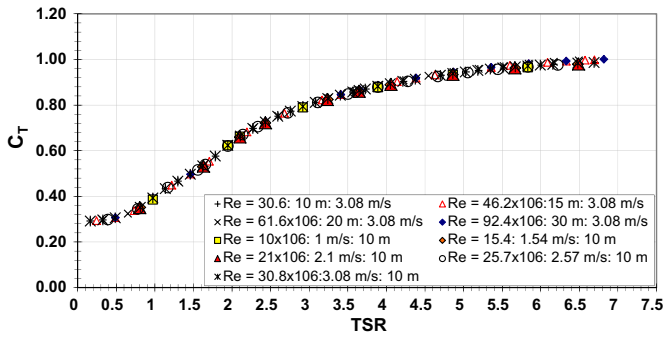


Fig. 13. Combined axial thrust coefficient ( $C_T$ ) vs TSR with increasing turbine diameter and upstream water velocity (uniform flow = 3.08 m/s for diameters 10 m–30 m).

TSR for the same range of diameters and velocities yield single curves, illustrating that the turbine has a unique torque/axial thrust-TSR characteristics that are independent of Reynolds number, for the range considered.

Large turbines will inevitably have large Reynolds numbers, but small experimental turbines will have much lower values. Tedds et al. [2] presented experimental data of  $C_p$  vs TSR which showed that their 0.5 m experimental turbine did not exhibit Reynolds number independence for inlet velocities below about 1 m/s, which corresponds to a Reynolds number based on the turbine diameter of  $5 \times 10^5$ . Fig. 14 shows the effect of Reynolds number as predicted by the CFD; the graph is charting the decrease of the peak values of  $C_p$  and  $C_\theta$  (i.e. the maximum values in Figs. 11 and 12) as Reynolds number is increased. Consistent with the data of Tedds et al. [2], it can be seen that Reynolds number insensitivity is achieved at a Reynolds number of  $5 \times 10^5$ , although  $3 \times 10^5$  could also be taken as the critical Reynolds number; to put this into perspective, a 10 m diameter turbine in a 1 m/s flow will have a Reynolds number of  $1 \times 10^7$ . This is a very useful design guide for experimentalists and although the value is only strictly applicable to this design of turbine, it can still be expected to be a good guide for other HATTS, although other designs of turbines will exhibit their own critical Reynolds number.

4.2. CFD predictions for non-uniform velocity profile

To determine the effect of a non-uniform inlet flow, a velocity profile based on the data recorded at a location within the Severn Estuary, by an ADCP system, was used [18]. The water depth at this location was 35 m (LAT). Due to the shipping restrictions within the Severn Estuary, HATT diameters greater than 15 m would exceed the limited depth clearance between the maximum vessel hull depth for the location and the tip of the turbine while at the top of its rotation cycle. Given these restrictions, the diameter of the HATT was set at 10 m, as this gave the hull clearance required. Moreover, due to the rapid decay in the velocity profile toward the seabed the HATT rotation axis was raised to a height, given the restrictions

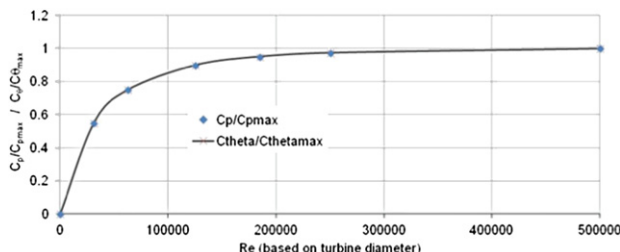


Fig. 14. Effect of Reynolds number on turbine characteristics.

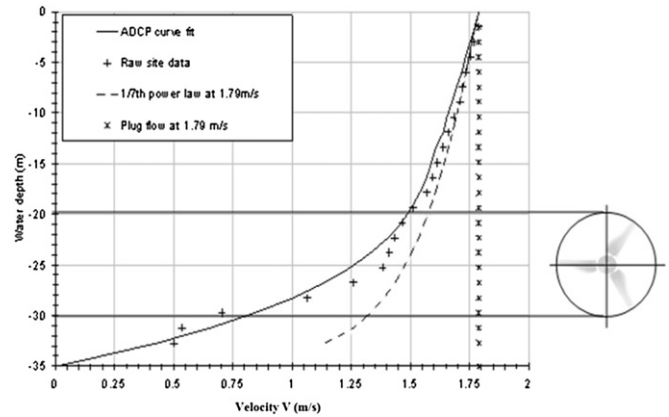


Fig. 15. Location of the HATT in a non-uniform velocity profile (ADCP measured).

discussed above, of 10 m above the seabed. This meant the turbine was within the lowest 25% of the water depth. The velocity profile through the water column is shown in Fig. 15. Also included in Fig. 15 is the uniform (or plug) flow profile at the peak velocity, the commonly used 1/7th profile (for comparison) and the location of the 10 m diameter turbine used in the CFD calculations.

Figs. 11–13 demonstrated that for a turbine of a particular geometry operating in a current with a uniform inlet velocity profile, the turbine output characteristics are unique functions of TSR. However, as discussed earlier, in reality the velocity profile through the water column is far from uniform. Because the available power is proportional to the cube of the velocity, the reduced velocity at depth will have a significant effect on the amount of power that can be extracted, and on the economic viability of a particular installation. Dimensional analysis requires both geometric and dynamic similarity so that scaling between different conditions remains valid. In the case of a non-uniform velocity profile the analysis requires a characteristic velocity to effectively represent the flow velocity. The logical choice for a characteristic velocity is a mean value and for the sake of comparison the average firstly based on the volume flow through the circle prescribed by the turbine (i.e volume flow rate divided by area)  $V_v$ , and secondly the depth averaged velocity across the vertical diameter of the turbine,  $V_d$  were used.

Referring to Fig. 15, the ADCP velocity profile can be seen to vary significantly across the diameter of the turbine. The volume-averaged velocity,  $V_v$ , is calculated by integrating the velocity profile across the face of the turbine, assuming the velocities do not change in the horizontal direction, to give the volume flow rate; this is

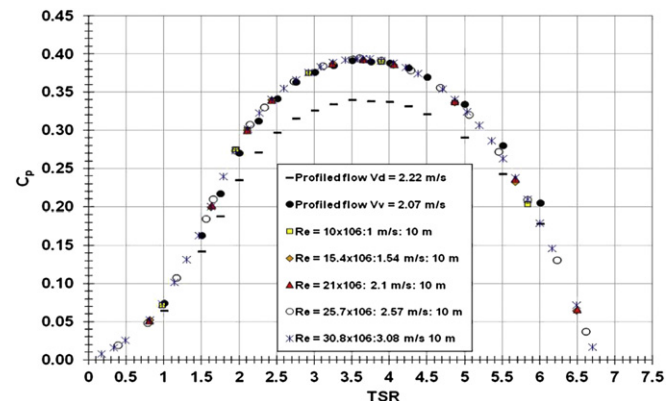


Fig. 16. Power coefficient ( $C_p$ ) vs TSR with increasing upstream water velocity (uniform) and average profiled flow across the turbine diameter.

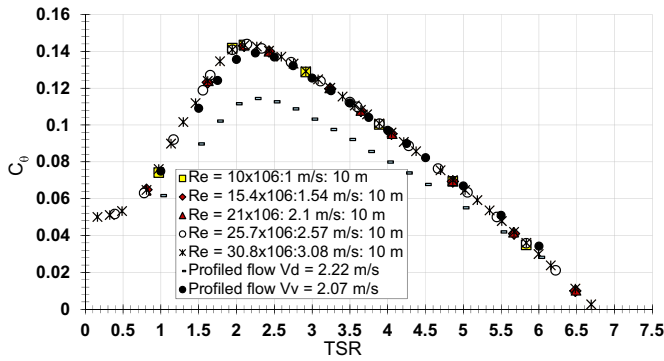


Fig. 17. Torque coefficient ( $C_0$ ) vs TSR with increasing upstream water velocity (uniform) and average profiled across the turbine diameter.

then divided by the frontal area of the turbine and, for the data shown in Fig. 15,  $V_v = 1.2$  m/s. Taking a simple average velocity across the vertical diameter, on the other hand, gives  $V_d = 1.28$  m/s.

Figs. 16–18 show the dimensionless characteristic curves for  $C_p$ ,  $C_0$  and  $C_T$  for a HATT with a uniform upstream water velocity together with the CFD-generated data calculated with the non-uniform velocity profile and represented by non-dimensional coefficients that have been calculated using both  $V_v$  and  $V_d$ . It can clearly be seen that the data, when expressed using the volume-averaged velocity, collapse onto the same curve as that produced using a uniform velocity profile. This is an important result as it means that turbine characteristics which have been obtained using uniform velocity profiles, either by experiment or CFD, can be corrected to account for depth-varying velocity profiles. A corollary is that if a turbine's performance is known for a given velocity profile, then it can be corrected for another profile, which will greatly assist in the evaluation of turbine performance for different locations.

It is useful to consider the velocities and turbine diameter shown in Fig. 15 to understand the magnitudes involved. The peak power coefficient of the turbine is 0.4 and if it was assumed that the surface velocity, 1.79 m/s, prevailed throughout the water column then this would yield a power output of 92.3 kW. However the actual power output, allowing for the velocity profile by using  $V_v = 1.2$  m/s, is 27.8 kW, less than a third of that calculated using just the surface velocity. Clearly, it is essential that the available power resource at any site is correctly evaluated. It is also interesting to note how low the power output is for this site in the Severn, thereby demonstrating why it is not considered as a prime site.

4.3. Non-dimensional study for reference CFD models with changes in blade pitch angle

Fig. 19 shows the effect of blade pitch angle variation on  $C_p$ . The 6° blade pitch angle follows the  $C_p$  curve in Fig. 11, whilst for angles

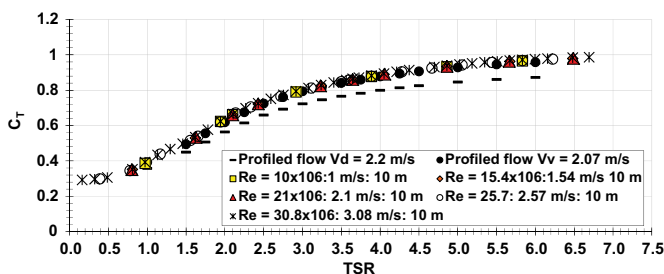


Fig. 18. Axial thrust coefficient ( $C_T$ ) vs TSR with increasing upstream water velocity (uniform) and average profiled across the turbine diameter.

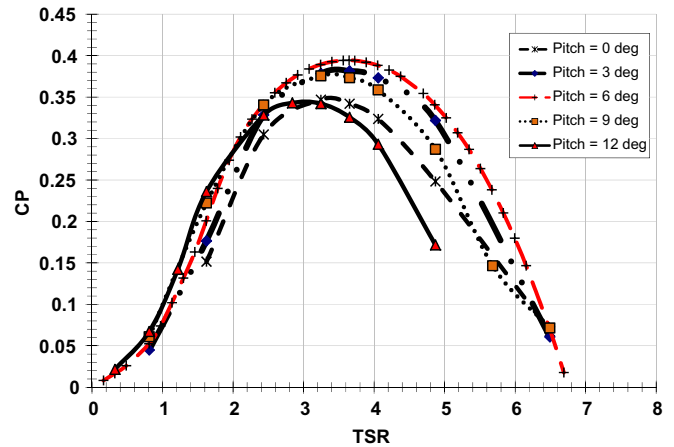


Fig. 19. Effect of blade pitch angle on  $C_p$  (uniform flow  $V = 3.08$  m/s).

of 0°, 3°, 9° and 12° there is a shift in the point of maximum power extraction and in the operational TSR range. This clearly demonstrates that the value of  $C_p$  can only be used for geometrically similar turbines, and any change in geometry leads to a new function  $f$  (equation (6)). Similarly, it can be seen in Fig. 20 that the value for  $C_0$  can also only be applied when geometric similarity is maintained, and that when the blade pitch angle is changed, a new function  $f_1$  is required. Fig. 20 shows an increase in peak  $C_0$  with blade pitch angles of 9° and 12° while operating at lower TSRs than those at 6°, 3° and 0°. The pitch angles of 9° and 12° show a higher start-up torque, which would allow the turbine to operate in slower moving water.

Fig. 21 shows the effect of the blade pitch angle on  $C_T$ . What is very clear from these curves is that, whilst  $C_p$  and  $C_0$  are reasonably insensitive to a change in the blade pitch angle  $\pm 3^\circ$  ( $C_p = \sim 6\%$  and  $C_0 = \sim 6\%$ ), the same cannot be said for the axial thrust. A variation of  $\pm 3^\circ$  from the optimum angle can either reduce  $C_T$  to 0.6 or increase it to 1.1. This could obviously have serious consequences on the integrity of the turbine structure. Using Figs. 19 and 21, the designer can make a judgement between adjusting the blade angle to reduce the axial load and the associated cost in power output. For example at peak power a 3° increase in the blade pitch angle (over the optimal 6°) would result in a 14% reduction in axial load for only a 6% reduction in power. It should be borne in mind, however, that these curves are for uniform velocity profiles and the previous discussion on the effect of velocity profile would have to be

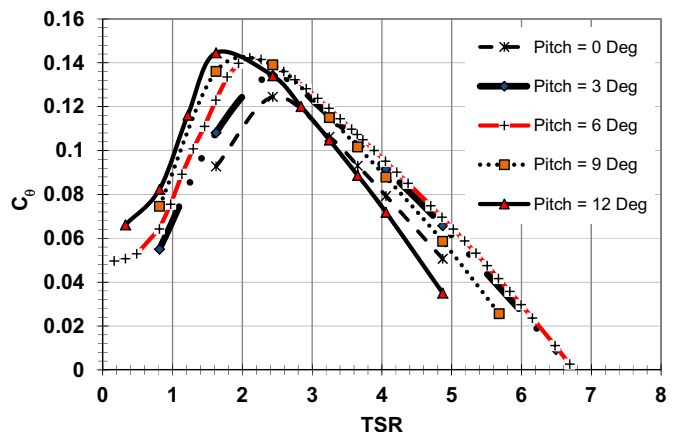


Fig. 20. Effect of blade pitch angle on  $C_0$  (uniform flow  $V = 3.08$  m/s).

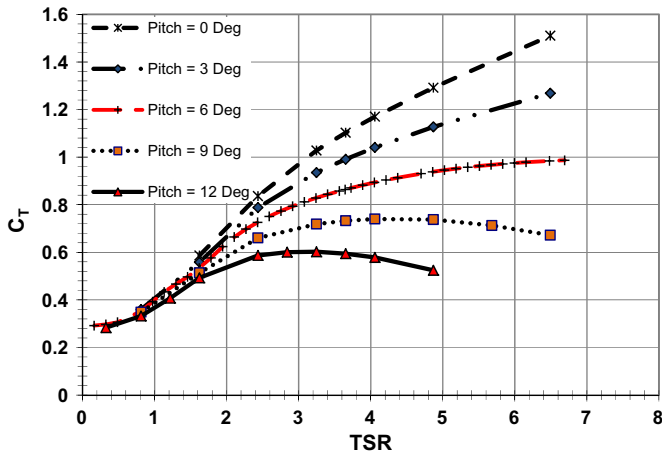


Fig. 21. Effect of blade pitch angle on  $C_T$  (uniform flow  $V = 3.08$  m/s).

considered. In the case of a velocity profile, the turbine's performance coefficients will fall within 2% of those predicted from a uniform velocity profile if the volumetric flow rate over the turbine's swept area is used. Hence, changes in the characteristics would also be expected for the non-uniform velocity profiles. However, since the terms are a function of  $V^2$  (torque and axial load) and  $V^3$  (power) then the coefficients are very sensitive to the accuracy of the calculated velocity.

If the models for the different pitch angles are run with  $V_v$  as the average velocity across the swept area, the results overlay those shown in Figs. 19–21.

## 5. Performance charts for prototype HATT design

In Section 4 it has been demonstrated that a particular design of HATT can be uniquely characterised by dimensionless parameters, which can be quantified by experiment or CFD, provided the Reynolds number (based on turbine diameter) is greater than  $5 \times 10^5$ . The dimensionless characteristics can be applied to geometrically similar turbines, of different size, deployed in tidal currents with uniform or non-uniform velocity profiles, provided the volume-averaged velocity is used.

Given the location discussed earlier for the HATT within the Severn Estuary and the restrictions imposed at the site due to local shipping lines, both the diameter and operational depth of the HATT are to some extent fixed. This type of restriction may well be a common problem at other sites especially if and when the technology is expanded. Bearing in mind that the appropriate characteristic velocity for the turbine is the volume-averaged value, a minimum value of 1.54 m/s was chosen as the minimum inlet velocity, which is just above the recommended minimum cut-in flow velocity of 1 m/s [10]. Fig. 22 has been constructed for the turbine configuration used in this study and for the given velocity range, using the optimum values of  $C_p$  and TSR of 0.4 and 3.6 respectively from Fig. 11, and using volume-averaged inlet velocities between 1.54 m/s and 3.086 m/s (3–6 knots) for a turbine diameter range between 6 m and 30 m. Using Fig. 22, it can be shown that to produce a rated power of 1 MW with the existing HATT design and a single rotor, a diameter of 15 m would be required for a velocity of 3.08 m/s. At a mean spring peak velocity of 2.57 m/s, typically discussed in literature, a diameter of approximately 18 m would be required. Again, it should be remembered that it is volume-averaged velocities that are being discussed.

The introduction of a velocity profile through the water column has a significant effect on power attenuation through the water depth. The cube proportionality on the velocity component will significantly affect power extraction estimates when using near surface measurements. Large velocity and shear rates towards the seabed therefore have the potential to compromise the operation of the turbine. As in the case of the Severn Estuary it is more than likely that the rotational axis depth of the turbine will be greatly influenced by local shipping restrictions. Using the scaling curves of Fig. 22 two rotors would be required with diameters of between 15 m and 20 m to meet the 1 MW target typically quoted. For a large part of the Severn Estuary it is more likely, due to large hull depth, that a turbine diameter would be restricted to around 10 m or less. Under these circumstances groups of between 4 and 6 turbines would be necessary. Under these circumstances, and using the findings of O'Doherty et al. [19,20], the spatial requirements for groups or arrays of turbines can clearly be predetermined.

The principle of this work has shown that only a single set of characteristic curves are needed in order to characterise the performance of a specified turbine blade design. However,

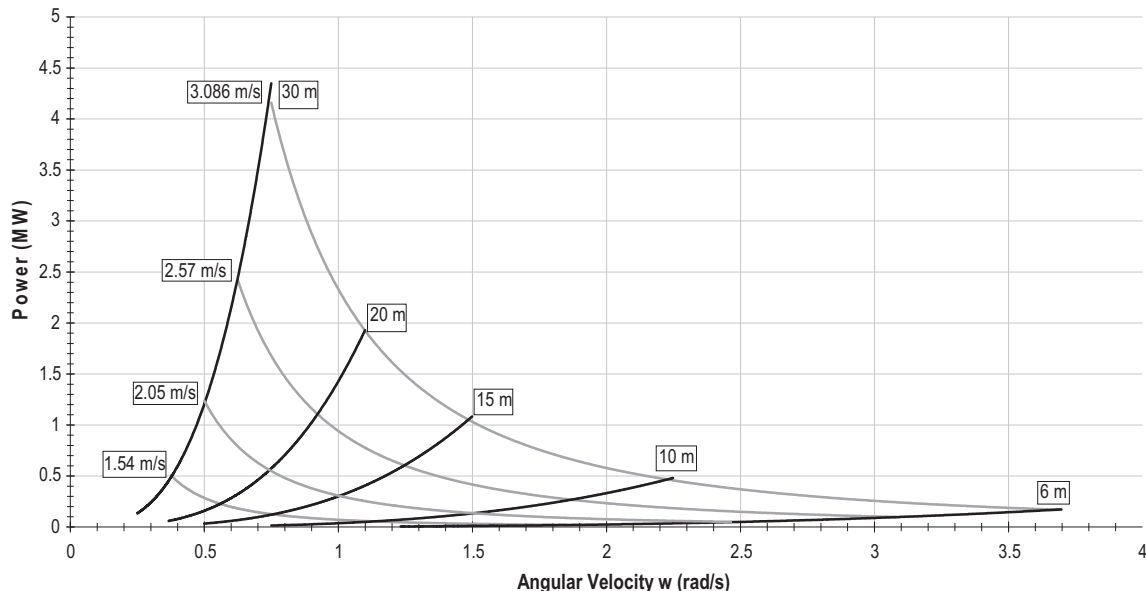


Fig. 22. Design specific peak power curves with increasing diameter and tidal velocity with a maximum tidal velocity of 3.08 m/s [16].

a variation in geometry, such as, the blade pitch angle would require a new set of curves.

## 6. Conclusion

It has been demonstrated that the performance characteristics of a HATT can be uniquely quantified by non-dimensional parameters and, for Reynolds numbers in excess of  $5 \times 10^5$ , the non-dimensional characteristics are independent of Reynolds number, for the particular geometry used in this study. In tidal currents that have a non-uniform profile, the non-dimensional characteristics are maintained if the volume-averaged velocity across the face of the turbine is used. Consistent with non-dimensional theory, it has also been shown that the dimensionless characteristics change when the turbine geometry is changed for uniform profiles and expected to be true for non-uniform profiles using the volume-averaged velocity.

## Acknowledgments

Low Carbon Research Institution (LCRI) for funding the work package. Also, thanks to Paul Malpas and Gareth Hunt for the design/manufacture of the nacelle housing and support plus instrumentation.

## References

- [1] Bahaj AS, Molland AF, Chaplin JR, Batten WMJ. Power and thrust measurements of marine current turbines under various hydrodynamic flow conditions in a cavitation tunnel and a towing tank. *Renewable Energy* 2006;32(No. 32):407–26.
- [2] Tedds SC, Poole RJ, Owen I, Najafian G, Bode SP, Mason-Jones A, et al. Experimental investigation of horizontal axis tidal stream turbines. 9th European Wave and Tidal Energy Conference (EWTEC), Southampton, UK; 2011.
- [3] O'Doherty T, Mason-Jones A, O'Doherty DM, Byrne CB, Owen I, Wang Y. Experimental and computational analysis of a model horizontal axis tidal turbine. 8th European Wave and Tidal Energy Conference (EWTEC), Uppsala, Sweden; 2009.
- [4] Batten WMJ, Bahaj AS, Molland AF, Chaplin JR. The prediction of the hydrodynamic performance of marine current turbines. *Renewable Energy* 2008;33: 1085–96.
- [5] Bryden IG, Naik S, Fraenkel P, Bullen CR. Matching tidal current plants to local flow conditions. *Energy* 1998;Vol. 23(No. 9):699–709.
- [6] Fraenkel. Under water windmills, Harnessing the World's marine currents. *INGENIA*, Issue 46, March 2011, [www.ingenia.org.uk/ingenia/issues/issue46/fraenkel.pdf](http://www.ingenia.org.uk/ingenia/issues/issue46/fraenkel.pdf); 8, April, 2011.
- [7] Auld T. (TAuld@abports.co.uk), (2008). Vessel draft. 20th March. Forwarded Email from: Evans, P., School of Earth, Ocean and Planetary Sciences, Cardiff University.
- [8] Hardisty J. Power intermittency, redundancy and tidal phasing around the United Kingdom. *The Geographical Journal* 2008;174(No. 1):76–84.
- [9] DTI. Economic viability of a simple tidal stream energy capture device; 2007. DTI project No. TP/3/ERG/6/1/15527/REP URN 07/575.
- [10] Black and Veatch. Tidal stream energy resource and technology summary report. Carbon Trust; 2005.
- [11] Batten WMJ, Bahaj AS, Molland AF, Chaplin JR. Experimentally validated numerical method for the hydrodynamic design of horizontal axis tidal turbines. *Ocean Engineering* 2007;34(7). ISSN: 00298018:1013–20. [doi:10.1016/j.oceaneng.2006.04.008](https://doi.org/10.1016/j.oceaneng.2006.04.008).
- [12] Whelan JI, Graham JMR, Peiro J. A free-surface and blockage correction for tidal turbines. *Journal of Fluid Mechanics* 2009;624:281–91.
- [13] Chen TY, Liou LR. Blockage corrections in wind tunnel tests of small horizontal-axis wind turbines. *Experimental Thermal and Fluid Science* 2011; 35(No. 3):565–9.
- [14] Millward A, Rossiter J. The design of a multi-purpose multicomponent strain gauge dynamometer. *Strain* 1983;19:27–30. [doi:10.1111/j.1475-1305.1983.tb00437.x](https://doi.org/10.1111/j.1475-1305.1983.tb00437.x).
- [15] Chaney K, Eggers AJ. Expanding wake induction effects on thrust distribution on a rotor disc. *Wind Energy* 2001;5:213–26.
- [16] Mason-Jones A. 2010. Performance assessment of a horizontal axis tidal turbine in a high velocity shear environment. PhD Thesis, Cardiff University, UK.
- [17] Fluent Inc.. Fluent documentation; 2006.
- [18] O'Doherty T, Mason-Jones A, O'Doherty DM, Evans PS, Wooldridge CF, Fryett I. An assessment of horizontal axis tidal turbines Sited off the Welsh Coast using ADCP and CFD analysis. *Proc. Inst of Civil Engineers. Energy* 2010;163: 1751–4223. EN3, ISSN.
- [19] O'Doherty T, Egarr DA, Mason-Jones A, O'Doherty DM. An assessment of axial loading on a 5 turbine array. *Proceedings of the Institute of Civil Engineers (ICE). Energy* 2009;162. EN2, ISSN.
- [20] O'Doherty DM, Mason-Jones A, Morris C, O'Doherty T, Byrne C, Prickett PW, et al. Interaction of marine turbines in close Proximity. 9th European wave and tidal energy Conference (EWTEC), Southampton, UK; 2011.